

Dynamics of domain wall driven by spin-transfer torque

P. Chureemart,* R. F. L. Evans, and R. W. Chantrell

Department of Physics, University of York, York YO10 5DD, United Kingdom

(Received 11 February 2011; revised manuscript received 28 March 2011; published 18 May 2011)

Spin-torque switching of magnetic devices offers new technological possibilities for data storage and integrated circuits. We have investigated domain-wall motion in a ferromagnetic thin film driven by a spin-polarized current using an atomistic spin model with a modified Landau-Lifshitz-Gilbert equation including the effect of the spin-transfer torque. The presence of the spin-transfer torque is shown to create an out-of-plane domain wall, in contrast to the external-field-driven case where an in-plane wall is found. We have investigated the effect of the spin torque on domain-wall displacement, domain-wall velocity, and domain-wall width, as well as the equilibration time in the presence of the spin-transfer torque. We have shown that the minimum spin-current density, regarded as the critical value for domain-wall motion, decreases with increasing temperature.

DOI: [10.1103/PhysRevB.83.184416](https://doi.org/10.1103/PhysRevB.83.184416)

PACS number(s): 75.78.Fg, 75.60.Ch, 52.55.Wq, 75.70.Kw

I. INTRODUCTION

The dynamics of domain-wall (DW) motion have been extensively studied¹⁻⁹ due to relevant applications in DW-based magnetic devices such as race track memory^{10,11} and logical operation in devices such as magnetic random access memory (MRAM).^{12,13} In conventional measurements of *field-induced* domain-wall motion, the domain wall is manipulated by applying an external magnetic field leading to deformation of the domain wall. However, this magnetic field usually covers a large spatial area, constraining the device design. Recently, a new concept to control the magnetic domain wall, called *current-induced* domain-wall motion, has attracted considerable attention in both theoretical and experimental studies.^{4-6,14,15} The phenomenon of spin-transfer torque (STT), which induces magnetization reversal and magnetic domain-wall motion, was first predicted by Berger¹⁶ and Slonczewski.¹⁷ This phenomenon has been widely studied in terms of numerous applications by many research groups; for a review, see Ref. 18.

The mechanism of spin torque involves the *s-d* exchange interaction between the nonequilibrium conduction electrons and the local magnetization of the ferromagnetic layer. Consider a trilayer structure of a pinned ferromagnetic layer separated from a free magnetic layer by a nonmagnetic conductor. Initially a current is injected into the pinned ferromagnetic layer causing it to be polarized. Subsequently, the spin-polarized current flows through the free layer and the spin-transfer torque acts on the spin current to align it in the direction of the free-layer magnetization. Simultaneously, a reaction torque is exerted on the magnetization of the free layer, causing magnetization reorientation. Complete magnetization reversal can occur in the case of a sufficiently large spin-current density. The key advantage of this technique is that the current-induced magnetization reversal can be confined to a small spatial area leading to many potential applications.

In this work, we study the trilayer magnetic system consisting of two ferromagnets separated by a nonmagnetic spacer layer. We investigate not only the effect of the spin-polarized current on the dynamics of the magnetization in a single domain wall of the free layer, but also the complicated dynamic behavior of the response of the domain-wall displacement due to the spin-transfer torques. The usual Landau-Lifshitz-Gilbert

(LLG) equation of motion at the atomistic level is modified by including the effect of the spin-transfer torque. The new modified LLG equation¹⁹⁻²¹ is used to describe the behavior of the domain wall for the trilayer geometry with dimensions for the free layer of $22 \times 22 \times 1$ nm. We show that the spin-transfer torque can influence the magnetic system by simultaneously behaving as an additional effective field and an additional damping term.

Current-induced domain-wall motion is studied by injecting a current with different magnitudes perpendicular to the plane of the trilayer. This allows the investigation of effects such as the critical current density (the minimum spin current required to move the domain wall), domain-wall displacement, domain-wall velocity, and domain-wall width, as well as the equilibration time for the magnetization reversal. Furthermore, the effects of thermal fluctuations on the critical spin-current density are also investigated and show a decreasing in the critical current density with increasing temperature.

II. ATOMISTIC MODEL

A. The classical spin Hamiltonian

The spin system is modeled using a classical spin Hamiltonian, with the parameters of cobalt. The classical spin Hamiltonian using the Heisenberg form of exchange can be written as

$$\mathcal{H} = - \sum_{i \neq j} J_{ij} \mathbf{S}_i \cdot \mathbf{S}_j - K_1 \sum_i (\mathbf{S}_i^2 \cdot \mathbf{e}^2) - \mu_s \cdot \mathbf{H}_{\text{applied}} \sum_i \mathbf{S}_i, \quad (1)$$

with the corresponding parameters expressed as energies per atom. Here, J_{ij} is the nearest-neighbor exchange integral between the spin site i and j , \mathbf{S}_i is the local normalized spin moment, \mathbf{S}_j is the normalized spin moment of the neighboring atom at site j , K_1 is the uniaxial anisotropy constant, \mathbf{e} is the unit vector of the easy axis, and $|\mu_s|$ is the magnitude of the spin moment. From the experimental value of T_c for Co, we take a value of $J_{ij} = 1.12 \times 10^{-20}$ J/link and the spin moment is taken as $|\mu_s| = 1.44 \mu_B$. The spin Hamiltonian represents the energies in the magnetic system including the exchange energy in the first term, the anisotropy energy, and the external

applied field, respectively. The inclusion of the demagnetizing field is determined separately in order to reduce the CPU time for the calculation by using a technique developed by Boerner *et al.*²² This approach proceeds by first dividing the thin sample into many small cells known as a “supercell.” The magnetic moment in each supercell is then calculated by averaging over the spins within the cell. Finally, the averaged moments are used to calculate the local dipolar field within each cell, which is taken as representative of all spins within that cell. The field is given by

$$\mathbf{H}_{\text{demag},i} = \frac{\mu_0 |\mu_s|}{4\pi} \sum_{i \neq j} \left[\frac{3(\mu_j \cdot \mathbf{r}_{ij})\mathbf{r}_{ij} - \mu_j}{|\mathbf{r}_{ij}|^3} \right], \quad (2)$$

and

$$\mu_j = \sum \mathbf{S}_j, \quad (3)$$

where μ_j is the unit vector of the magnetic moment at the supercell site j , which is found from the summation of spin moments in cell of the supercell j ; $|\mu_s|$ is the magnitude of the spin moment; μ_0 is the permeability of free space; and $|\mathbf{r}_{ij}|$ and \mathbf{r}_{ij} are the distance and unit vector, respectively, between supercell sites.

The thermal fluctuations are taken into account in the atomistic model using Langevin dynamics in the formalism of Brown,²³ under the assumption that the inclusion of temperature can be represented by a random field term.^{24,25} The statistical properties of the random field are described by using the fluctuation-dissipation theorem (FDT) and Fokker-Planck equation, and are given by the following equation:

$$\begin{aligned} \langle \zeta_i(t) \rangle &= 0, \\ \langle \zeta_i(t) \zeta_j(t') \rangle &= \delta_{ij} \delta(t - t') 2\alpha k_B T / (|\mu_s| \gamma), \end{aligned} \quad (4)$$

where i, j are the Cartesian components, ζ is a random field with Gaussian fluctuations, δ_{ij} is the Kronecker delta, $\delta(t - t')$ is the Dirac delta function, $2\alpha k_B T / (|\mu_s| \gamma)$ is the factor measuring the strength of thermal fluctuation, k_B is the Boltzmann constant, T is the system temperature in Kelvin, α is the damping parameter, and γ is the absolute value of the gyromagnetic ratio. In this paper, we use $\gamma = 1.76 \times 10^{11} \text{ s}^{-1} \text{ T}^{-1}$, and the units of μ_s are in joules per tesla (J T^{-1}).

The effective local field acting on spin site i in the atomistic model is given by

$$\mathbf{H}_{\text{eff}} = -\frac{1}{|\mu_s|} \frac{\partial \mathcal{H}}{\partial \mathbf{S}_i} + \mathbf{H}_{\text{demag},i} + \zeta_i(t). \quad (5)$$

B. The LLG equation with spin-transfer torque

To investigate the effect of the spin-transfer torque in the atomistic model, a trilayer structure is considered. The first ferromagnetic material is taken as a “pinned layer,” which gives rise to a spin-polarized current by virtue of the s - d exchange interaction. The resulting polarized spins then flow into the second (free) layer passing through the spacer layer, retaining an average polarized spin parallel to the magnetic moment in the pinned layer. These polarized spins will then interact with the magnetic moments in the free layer, finally giving absorption of the transverse component of the polarized spins in the free layer as the orientation of the spin current

rotates toward the direction of the free-layer magnetization. This gives rise to a torque exerted on the magnetic moments of the free layer to conserve the angular momentum, and this torque tends to reorient the magnetic moments in the free layer toward the incoming polarized spin alignment, which is parallel to the pinned layer.

In order to determine the dynamic motion of the magnetization, all torques acting on the magnetization in the free layer will be taken into account in the atomistic model through the modified LLG equation. In this paper, the spin-torque effect will be represented by an additional term added to the standard Landau-Lifshitz equation, based on the work of S. Zhang *et al.*^{4-6,19} as follows:

$$\frac{\partial \vec{S}}{\partial t} = -\gamma \vec{S} \times \mathbf{H}_{\text{eff}} + \frac{\alpha}{\mu_s} \vec{S} \times \frac{\partial \vec{S}}{\partial t} + \frac{\gamma a_j}{\mu_s} \vec{S} \times (\vec{S} \times \mathbf{S}_p), \quad (6)$$

where \vec{S} is the spin moment vector, \mathbf{S}_p is the normalized spin of the pinned layer, and a_j is the spin-torque parameter proportional to the injected current density. The spin motion as the above equation can be rewritten in terms of the normalized spin moment \mathbf{S} as

$$\frac{\partial \mathbf{S}}{\partial t} = -\gamma \mathbf{S} \times \mathbf{H}_{\text{eff}} + \alpha \mathbf{S} \times \frac{\partial \mathbf{S}}{\partial t} + \gamma a_j \mathbf{S} \times (\mathbf{S} \times \mathbf{S}_p). \quad (7)$$

For convenient numerical integration, Eq. (7) can be converted into the Landau-Lifshitz-Gilbert form by using the conservation of magnitude of magnetic moment, determining the cross product of the second term,

$$\begin{aligned} \mathbf{S} \times \frac{\partial \mathbf{S}}{\partial t} &= -\gamma \mathbf{S} \times (\mathbf{S} \times \mathbf{H}_{\text{eff}}) + \alpha \mathbf{S} \times \left(\mathbf{S} \times \frac{\partial \mathbf{S}}{\partial t} \right) \\ &\quad + \gamma a_j \mathbf{S} \times [\mathbf{S} \times (\mathbf{S} \times \mathbf{S}_p)], \end{aligned}$$

and subsequently,

$$\mathbf{S} \times \frac{\partial \mathbf{S}}{\partial t} = -\gamma \mathbf{S} \times (\mathbf{S} \times \mathbf{H}_{\text{eff}}) - \alpha \frac{\partial \mathbf{S}}{\partial t} - \gamma a_j (\mathbf{S} \times \mathbf{S}_p). \quad (8)$$

Substituting Eq. (8) into Eq. (7), we obtain the final form,

$$\begin{aligned} \frac{\partial \mathbf{S}}{\partial t} &= -\frac{\gamma}{(1 + \alpha^2)} \mathbf{S} \times \mathbf{H}_{\text{eff}} - \frac{\gamma \alpha}{(1 + \alpha^2)} [\mathbf{S} \times (\mathbf{S} \times \mathbf{H}_{\text{eff}})] \\ &\quad - \frac{\gamma \alpha a_j}{(1 + \alpha^2)} (\mathbf{S} \times \mathbf{S}_p) + \frac{\gamma a_j}{(1 + \alpha^2)} [\mathbf{S} \times (\mathbf{S} \times \mathbf{S}_p)]. \end{aligned} \quad (9)$$

The first two terms in Eq. (9) are the usual precessional and damping terms, which lead to damped precessional motion in the direction of the local field \mathbf{H}_{eff} . Furthermore, in the presence of an injected current, the last two terms, referred to as “the additional spin-torque terms,” describe the spin-torque effect on the spin motion. They indicate that the spin-torque term can be another source of precession and damping, due the third term in Eq. (9) acting as an effective field and the last term acting as a damping.^{4,26,27} The damping can be characterized by considering the direction of the damping term due to the spin-transfer torque, which is dependent on the direction of the injected current. If the damping torque term points in the same direction as the natural damping, there is enhanced effective damping giving the faster relaxation toward the effective field direction. However, the spin-transfer torque can

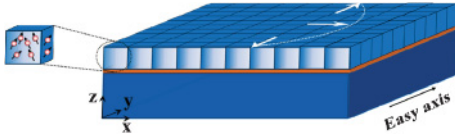


FIG. 1. (Color online) System geometry showing the zero-field equilibrium domain-wall structure: The trilayer structure consists of two ferromagnetic layers (top and bottom layers) separated by the spacer layer (middle layer). The free layer is divided into small cells to observe the domain-wall motion under different conditions. The white arrows show the tail-to-tail domain wall in the free layer with zero field and the easy axis is in the y direction.

act in the opposite direction to the damping term. This implies that the spin-transfer torque can either increase or decrease the natural damping of the spin motion depending on the direction of the injected current. The precessional states of the dynamic motion can be generally observed by the critical current density, which is the minimum value of the injected current leading to domain-wall motion.¹⁸

The modeled system consists of a single thin film of $100 \times 100 \times 5$ atoms. The atoms are assigned to cells with a size of $5 \times 5 \times 5$ atoms for the calculation of the demagnetization field, with the same supercell used to determine average magnetizations in order to quantify the dynamics of domain-wall motion. The system geometry is shown in Fig. 1, which also illustrates the zero-field equilibrium domain-wall structure. In order to force a domain wall into the film, at the boundaries corresponding to $y = 0$ and $y = L$, with L the in-plane size of the system, the spin direction is pinned along the $\pm y$ direction, respectively. We assume the presence of a first (pinned) layer. This layer is not considered explicitly; its role is simply to provide a spin-polarized current through the layer under investigation. The time evolution of the magnetization structure and the motion of the DW following the application of an external field or spin-polarized current is investigated by monitoring the magnetization of each grid point of the supercell.

In this computational study, we investigate the effect of the spin-transfer torque on the DW dynamics and the DW displacement, DW velocity, and DW width on time scales of the order of picoseconds. The time scales considered

here are very short due to the effect of the spin torque exerted on the local magnetization, which is in relation to most simulations and experiments.^{4,6,28} The investigation is presented in two sections. First we consider the nonthermal case, which demonstrates the critical field and current for DW motion and also interesting spin-torque oscillations in the equilibrium DW position. We then consider the case of a nonzero temperature, which leads to a variation in the critical current.

III. RESULTS

Initially we present a calculation of the DW width as a function of the uniaxial anisotropy constant in order to verify the atomistic calculations in relation to the continuum (micromagnetic) theory. The effective DW width (δ) in terms of the uniaxial anisotropy can be obtained using a micromagnetic approach as follows:²⁹

$$\delta = \pi \sqrt{\frac{A}{K_u}}, \quad (10)$$

where K_u is the uniaxial anisotropy constant and A is the exchange stiffness constant.

The studied system is based on the material properties of cobalt, i.e., a uniaxial anisotropy constant of $K_u = 4.18771 \times 10^5 \text{ J/m}^3$, with the y direction as the easy axis and an exchange stiffness constant of $A = 1.4 \times 10^{-11} \text{ J/m}$; see Fig. 2. In order to test the atomistic model, we first calculate the domain-wall width as a function of the anisotropy constant for comparison with the analytical expression. The domain walls are investigated by observing the magnetization components at any grid point of the domain wall. At the center of the DW, the x component of magnetization is maximum and the y component is zero, which is consistent with the formation of a Néel wall and a previous study of the similar system.⁷

The numerically calculated DW widths for different anisotropy constants are compared with the analytical solutions calculated from Eq. (10) in Fig. 3. As expected, the DW width decreases with increasing anisotropy constant, and the numerical solution is consistent with the analytical result. This represents a useful test of the atomistic model in its prediction of the static magnetic properties. It is likely that the calculated

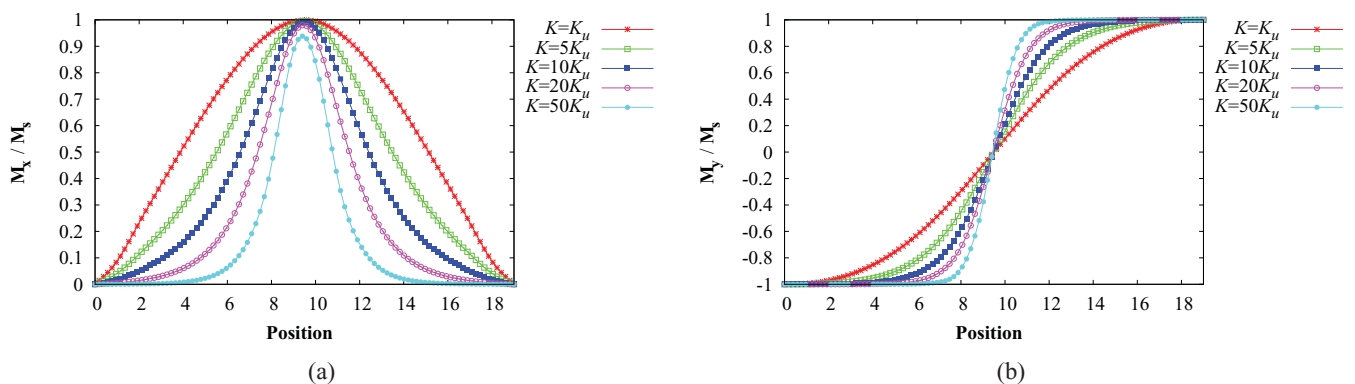


FIG. 2. (Color online) Atomistic calculation of the effect of different anisotropy constants on the domain-wall formations in zero field after 400 ps. The magnetization components (a) parallel and (b) perpendicular to the domain wall are shown. The distance is given in units of supercells, corresponding to 5 atomic spacings. Lines provide a guide to the eye.

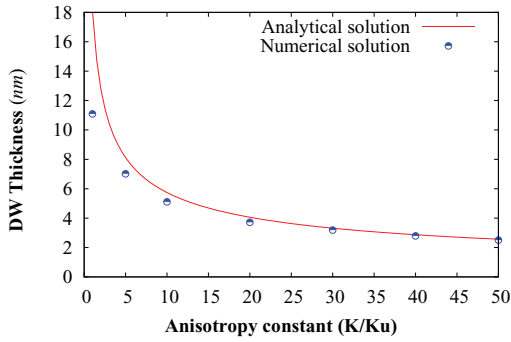


FIG. 3. (Color online) Domain-wall width vs anisotropy constant: Comparison between the analytical solution and the numerical solution.

domain-wall width for low anisotropy is lower than expected due to the finite system size and also a longer equilibration time than the simulation. From this point, the uniaxial anisotropy constant of $K_u = 4.2 \times 10^5 \text{ J/m}^3$ is chosen to apply for all the computational test systems.

A. Field-induced DW motion: Athermal case

We now present a study of domain-wall motion under the influence of an external field applied along the easy axis of the film. The first observation is the spatial dependence of the magnetization in order to determine the effect of the external field on the domain-wall motion. Results for the equilibrium wall position are shown in Fig. 4, where the position of the domain-wall center is in the middle of the sample in the absence of the applied field. In the presence of an applied field along the y direction, the domain-wall center moves to the left because the applied field tends to reorient the magnetization toward the field. The applied field induces a damped precessional motion resulting in motion of the domain wall.

Furthermore, the displacement and the velocity of the domain wall are monitored by observing the shift of the domain-wall center from the initial position at each time step. The relation between the domain-wall displacement and time evolution is plotted in Fig. 5(a). It can be seen that the domain-wall displacement is time dependent and oscillatory

with a frequency increasing with the applied field, eventually reaching a steady state with finite displacement.

On application of the external magnetic field, the spins in the domain wall tend to reorient toward the effective field direction, initiating domain-wall motion. The spins within the domain wall precess around the local minimum energy before reaching the equilibrium state, resulting in the oscillation of the displacement. As a result of the pinned boundaries, the partial magnetizations in the domain wall realigned in the y direction, resulting in a smaller domain-wall width, as shown in Fig. 4(a).

The velocity of the domain wall is then calculated by determining the rate of change of the domain-wall displacement. The variation of the DW velocity with time is shown in Fig. 5(b). It can be seen that the dynamic velocity is oscillatory and gradually decreases to zero at equilibrium. The initial velocities induced by the applied field can be used to evaluate the critical applied field, as shown in Fig. 6. The initial velocity is linearly proportional to the external magnetic field and gives an estimated critical field, initiating domain-wall motion at around 0.162 mT, which is very small compared to previous studies,^{30,31} where the critical field is around 4 mT. However, the critical field is inversely proportional to the damping constant and the saturation magnetization, and the previous studies investigated systems with low damping ($\alpha = 0.01$). At the value of damping constant used here of 0.1, the critical field should be an order of magnitude smaller, so our value of 0.162 mT is not unreasonable.

B. Spin-transfer-torque-induced DW motion: Athermal case

The next case of interest is the effect of the spin-transfer torque on the domain-wall motion by applying a spin current into the trilayer system. The resulting DW motion is observed through the components of the magnetization plotted in Fig. 7. This shows the magnetization components along the domain wall at 400 ps after the introduction of a spin torque, for different values of the spin-torque parameter a_j . Note first that this is a calculation assuming low anisotropy giving rise to a relatively wide DW with a width of approximately 11.088 nm in the case of zero current, and second that all nonzero values of a_j are greater than the critical value for DW motion to be considered later.

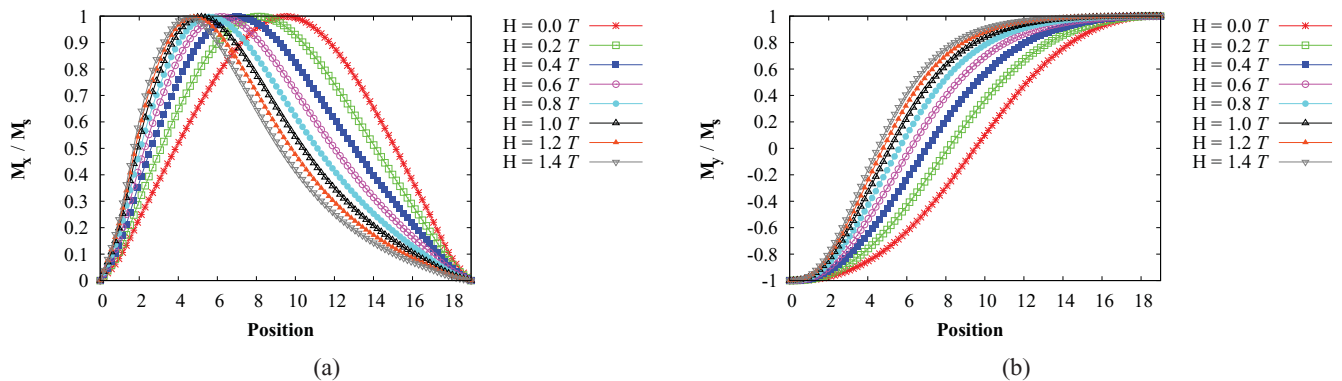


FIG. 4. (Color online) The effect of increased applied magnetic field on the domain-wall position (a) parallel and (b) perpendicular to the domain wall after 400 ps.

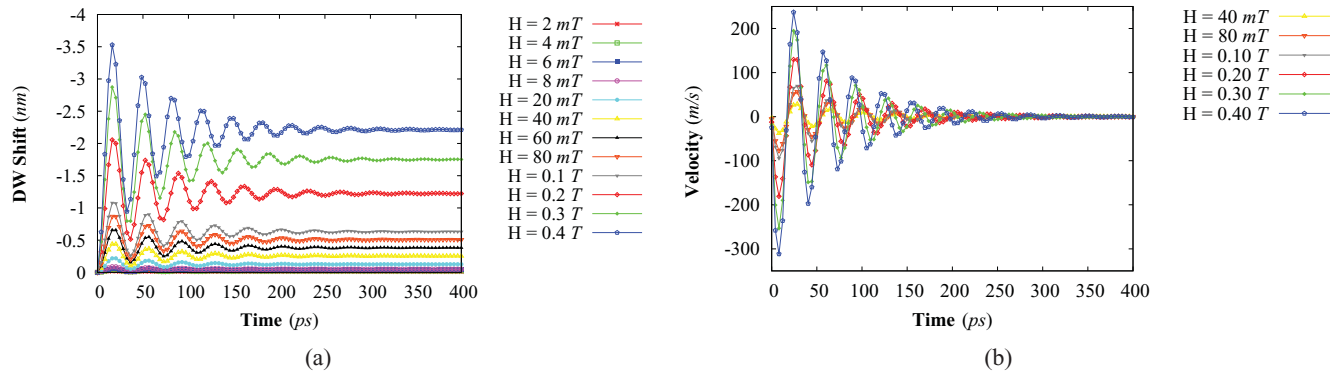


FIG. 5. (Color online) The time-dependent variation of the (a) domain-wall displacement and (b) domain-wall velocity for different applied magnetic fields.

In the absence of a spin torque, the DW is situated centrally, and the position of the domain-wall center is defined by the maximum magnetization of the x component and zero of the y component. When the spin current is injected, the center of the domain wall is moved, dependent on the relative orientation of the pinned layer and the free layer. Increasing the spin-current density represented by the spin-torque parameter (a_j) leads to a displacement of the domain-wall center along the direction of the spin-torque-induced field. In contrast, the domain wall can be moved in the opposite direction by applying the opposing spin current. The fixed boundary conditions at the edge of the system ensure that the domain wall is constrained within the system, with the boundary essentially behaving as a strong pinning site. Once domain-wall motion is initiated, the domain wall interacts with the strong pinning site so we are able to consider both the motion of the wall and its interaction with the pinning site. As the DW is forced against the pinning site, it is found that the width of the wall decreases. In addition, an out-of-plane component of magnetization appears due to the additional spin-transfer torque arising from the spin current. We note that Fig. 7 shows oscillatory behavior of the sign of m_z , with increasing a_j . This results from an induced precessional motion whose frequency depends on a_j . This is essentially a spin-torque-induced oscillation, which will be discussed later.

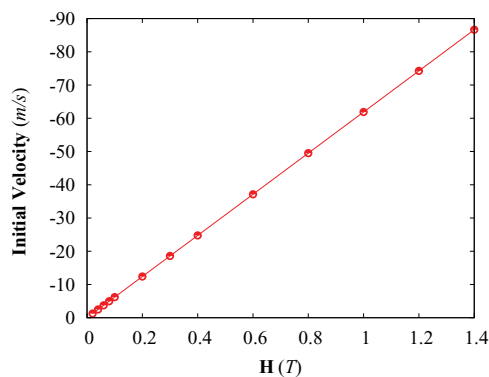


FIG. 6. (Color online) The initial velocities of the domain walls driven by different applied magnetic fields. The line is a fit to the data.

It is important to note a qualitative difference with the motion arising from the application of a static magnetic field. The application of a magnetic field induces a quasistatic shift of the DW position with time, with the sign of m_z unchanged. However, according to Fig. 7, the effect of the

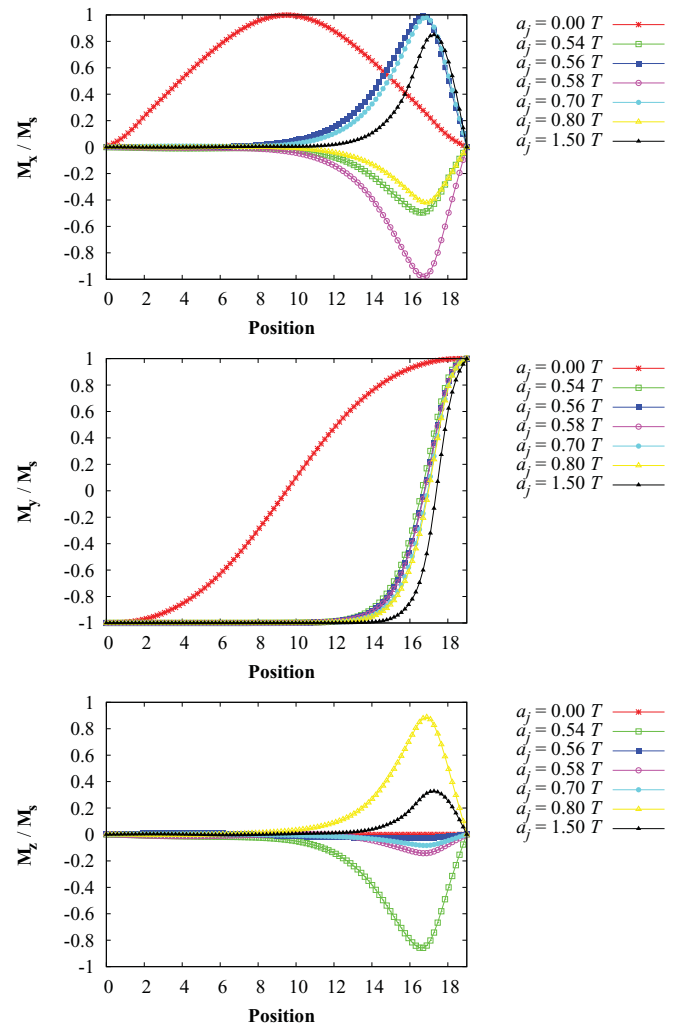


FIG. 7. (Color online) The magnetization components along the domain-wall direction 400 ps after the introduction of the spin torque for different values of the spin-torque parameter a_j . The distances are given in units of the supercell, corresponding to 5 atomic spacings.

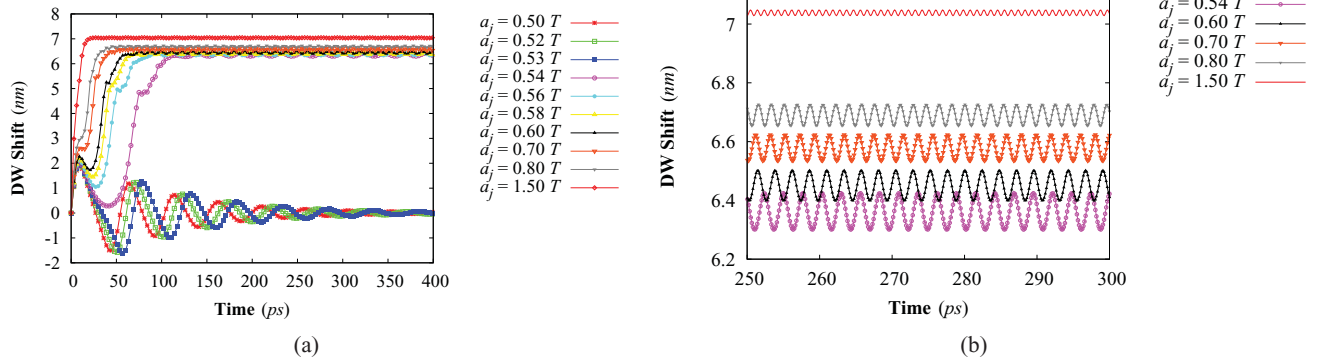


FIG. 8. (Color online) The time-dependent variation of the domain-wall displacement for (a) different current-induced magnetic fields (a_j) at zero temperature and (b) different spin-current densities of the time period 200–300 ps.

spin current is dramatically different even though the spin current is delivering an effective field similar in magnitude to the applied fields considered earlier. Specifically it can be seen that the sign of m_z oscillates with increasing current. This feature is ascribed to the “antidamping” effect of the spin torque, which counteracts the damping of the spin motion. In the case of the static applied field, the damping is sufficient to damp the precessional moment quickly enough so that m_z does not change sign. However, the antidamping introduced by the spin-torque term enhances the precessional motion to the extent that several cycles occur before equilibrium is established, leading to the oscillatory behavior of m_z evident in Fig. 7, in agreement with the previous studies.^{7,9} This is demonstrated in the time dependence of the domain-wall displacement, as shown in Fig. 8. The position of the domain wall is determined by the zero crossing of m_y . The results indicate a complex behavior on the subpicosecond time scale. In particular, there is a critical value of the spin-torque parameter a_j^{cr} below which DW motion is not initiated.

For a small spin-transfer torque $a_j < a_j^{cr}$, an overall domain-wall motion does not occur. However, the application of the spin torque does initiate dynamic motion of the domain-wall displacement, which is of an oscillatory nature, decaying as a damped sine function back to its initial position at equilibrium.

It can be concluded that the spin-transfer torque created by the spin current below the critical value has no influence

on the domain wall beyond this transient motion. On increasing the spin current, it can be seen that above a critical value determined as $a_j^{cr} = 0.54$ T, a net domain-wall motion is instigated. The value of $a_j^{cr} = 0.54$ T corresponds to the spin-current density of $j_e = 2.95 \times 10^{12}$ A/m². Below this critical value, the domain wall exhibits transient oscillatory behavior back to its initial position, as shown in Fig. 8(a).

In the case of injecting a spin-polarized current greater than the critical value, the dynamic behavior of the domain wall is also oscillatory, but exhibits a stable precessional state with a finite wall displacement, driven by the spin torque. With increasing spin-current density, the oscillation period decreases and the final precessional state is obtained more rapidly. Interestingly it can be seen that at equilibrium, the pinned domain wall essentially acts as a spin-torque oscillator. As a result of increasing the spin-current density, the oscillation frequency apparently increases, while the amplitude of oscillation decreases. This implies that the stable equilibrium state without precession can be achieved by the application of sufficiently large spin-current density, as shown in Fig. 8(b).

After applying the spin-polarized current, there is a spin-transfer torque acting on the DW, which results in DW motion and a smaller DW width compared to the initial state, as shown in Fig. 9. The change of DW width is brought about by the change in local field as the magnetization precesses out of plane. As a result, the DW width decreases with increasing spin-current density and also decreases with time. The vari-

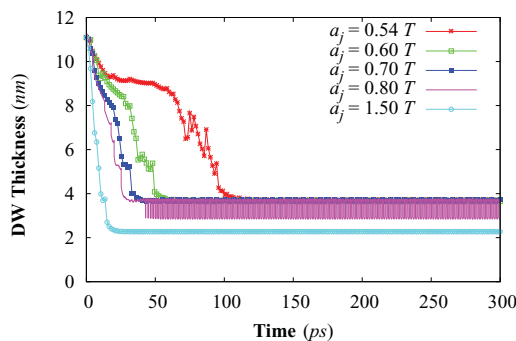


FIG. 9. (Color online) The time-dependent variation of the domain-wall width for different current-induced magnetic fields at zero temperature.

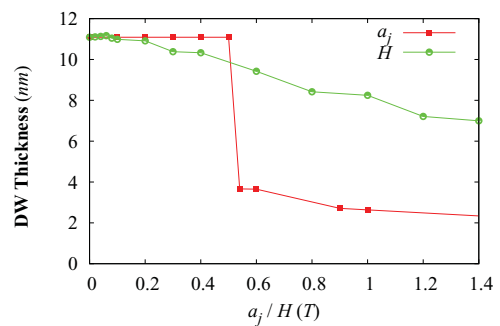


FIG. 10. (Color online) Comparison of the domain-wall width driven by the external magnetic field and the current-induced magnetic field at zero temperature.

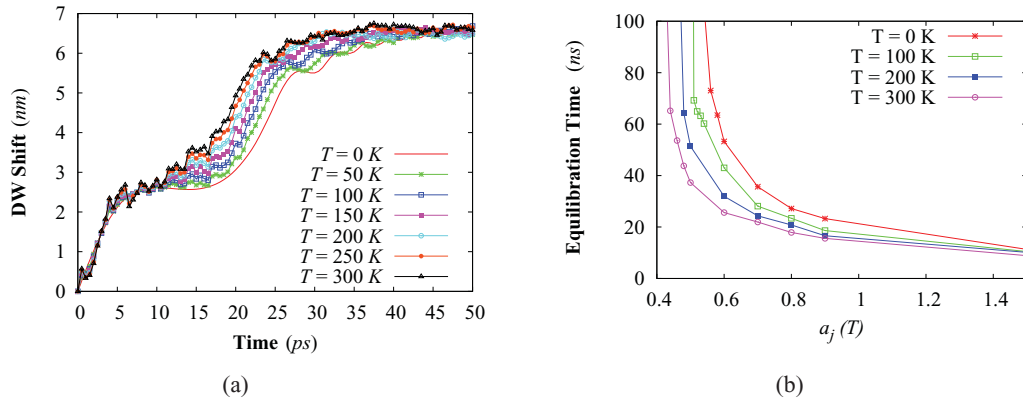


FIG. 11. (Color online) Temperature dependence of (a) the domain-wall displacement for $a_j = 0.7$ T and (b) the equilibration time for different values of the spin-torque parameter.

ation is a combination of the out-of-plane magnetization and the restriction of the wall due to the pinned magnetization. At equilibrium, the DW width oscillates slightly, driven by the spin torque.

It is also interesting to consider the equilibrium DW width as the wall is forced into contact with the pinning spins, particularly to compare the field- and spin-torque-driven cases. The DW width in these calculations is a good indicator of the final position of the wall in relation to the pinning sites. As noted previously, the DW width decreases as the wall is forced against the pinning sites. Figure 10 shows the calculated wall width at equilibrium for the field- and spin-torque-driven cases. In response to the external magnetic field, the DW width is still unchanged until the applied field reaches a critical applied field of 0.1616 mT and then varies continuously, with the field reflecting a gradual change of the DW position with increasing field. Similarly, the DW width of the test system with the spin-transfer torque remains constant for spin currents below a critical value, found to be 0.54 T. However, for a spin current greater than the critical value, the DW width in the spin-torque-driven case shows discontinuous behavior. This arises because of the fact that the enhanced precessional motion introduced by the spin torque results in an equilibrium state closer to the pinning site.

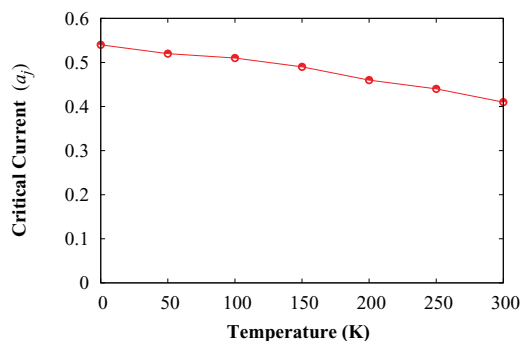


FIG. 12. (Color online) The critical spin-transfer-torque field for different temperatures.

C. Spin-transfer-torque-induced DW motion: Nonzero temperature case

We now consider the effect of thermal fluctuations in the atomistic model on the spin-transfer torque. The temperature dependence of the time to equilibrium is shown in Fig. 11(a) for a spin-torque parameter $a_j = 0.7$ T. For the first few picoseconds, the motion is largely independent of temperature, and the saturation value of the displacement is also temperature independent. However, in the range $5 < t < 30$ ps, the dynamics change systematically with temperature, exhibiting a reduction in the equilibration time. This arises due to the temperature-dependent magnetic properties, such as magnetization and anisotropy, leading to an increase in the effective damping, and therefore faster dynamic behavior. A systematic investigation of the equilibration time is shown in Fig. 11(b) for different temperatures as a function of the spin-torque parameter. It is defined as the consuming time of the system used to reach the final stable precessional state since the DW starts moving. At constant spin-transfer torque with varying temperature, it can be seen that the equilibration time decreases with increasing temperature. The equilibration time diverges at a critical value of a_j which characterizes the critical current for DW motion.

It is also interesting to investigate the temperature dependence of the critical spin-torque parameter, shown in Fig. 12. The data show a linear decrease of the critical field in the temperature range studied, probably due to a reduction in the anisotropy. This result is consistent with the experiments of Tsoi *et al.*³² showing that the critical current density for the initiation of DW motion decreases with temperature.

IV. CONCLUSIONS

Spin-torque-induced DW motion is a possible technique to control and manipulate the dynamics of the magnetization. We have investigated current-induced domain-wall motion theoretically using an atomistic model based on the modified LLG equation including the effect of the spin-transfer torque.

We have demonstrated the effects of spin torque on the dynamics of a domain-wall motion, demonstrating the appearance of an out-of-plane z component of the magnetization for

larger values of spin torque. We have investigated both the displacement of the domain wall and its interaction with a pinning site, and we have shown the existence of spin-torque oscillations driven by the polarized current. The dynamic response of the DW displacement is found to be nonlinearly dependent on time, especially in the case of the small spin current around the critical value of 0.54 T or $j_e = 2.95 \times 10^{12}$ A/m² for the athermal case. The wall displacement is found to be faster for larger values of the spin current. Moreover, we have found that the DW width is significantly reduced due to the spin current.

The inclusion of temperature effects has shown a linear decrease with temperature of the critical field for domain-wall motion, in agreement with the experimental data. This is an important consideration in the use of spin-torque switching, since the required high current densities result in significant heating and consequent temperature increase.

ACKNOWLEDGMENTS

P.C. gratefully acknowledges support from the Royal Thai Government.

*pc536@york.ac.uk

- ¹J. Xiao, A. Zangwill, and M. D. Stiles, *Phys. Rev. B* **72**, 014446 (2005).
- ²M. D. Stiles, W. M. Saslow, M. J. Donahue, and A. Zangwill, *Phys. Rev. B* **75**, 214423 (2007).
- ³S. Zhang and Z. Li, *Phys. Rev. Lett.* **93**, 127204 (2004).
- ⁴Z. Li and S. Zhang, *Phys. Rev. B* **68**, 024404 (2003).
- ⁵Z. Li and S. Zhang, *Phys. Rev. B* **70**, 024417 (2004).
- ⁶Z. Li and S. Zhang, *Phys. Rev. Lett.* **92**, 207203 (2004).
- ⁷A. Rebei and O. Mryasov, *Phys. Rev. B* **74**, 014412 (2006).
- ⁸A. V. Khvalkovskiy, K. A. Zvezdin, Y. V. Gorbunov, V. Cros, J. Grollier, A. Fert, and A. K. Zvezdin, *Phys. Rev. Lett.* **102**, 067206 (2009).
- ⁹C. T. Boone and I. N. Krivorotov, *Phys. Rev. Lett.* **104**, 167205 (2010).
- ¹⁰S. S. P. Parkin, M. Hayashi, and L. Thomas, *Science* **320**, 190 (2008).
- ¹¹L. Thomas, R. Moriya, C. Rettner, and S. S. Parkin, *Science* **330**, 1810 (2010).
- ¹²S. Tehrani *et al.*, *J. Appl. Phys.* **85**, 5822 (1999).
- ¹³H. Boeve *et al.*, *IEEE Trans. Magn.* **35**, 2820 (1999).
- ¹⁴J. Grollier *et al.*, *J. Appl. Phys.* **92**, 4825 (2002).
- ¹⁵M. Kläui, P.-O. Jubert, R. Allenspach, A. Bischof, J. A. C. Bland, G. Faini, U. Rüdiger, C. A. F. Vaz, L. Vila, and C. Vouille, *Phys. Rev. Lett.* **95**, 026601 (2005).
- ¹⁶L. Berger, *Phys. Rev. B* **54**, 9353 (1996).
- ¹⁷J. C. Slonczewski, *J. Magn. Magn. Mater.* **159**, L1 (1996).
- ¹⁸D. C. Ralph and M. D. Stiles, *J. Magn. Magn. Mater.* **320**, 1190 (2008).
- ¹⁹S. Zhang, P. M. Levy, and A. Fert, *Phys. Rev. Lett.* **88**, 236601 (2002).
- ²⁰P. M. Levy, *J. Phys. D* **35**, 2448 (2002).
- ²¹A. Shpiro, P. M. Levy, and S. Zhang, *Phys. Rev. B* **67**, 104430 (2003).
- ²²E. Boerner, O. Chubykalo-Fesenko, O. Mryasov, R. Chantrell, and O. Heinonen, *IEEE Trans. Magn.* **41**, 936 (2005).
- ²³W. F. Brown, *Phys. Rev.* **130**, 1677 (1963).
- ²⁴O. Chubykalo *et al.*, *J. Magn. Magn. Mater.* **266**, 28 (2003).
- ²⁵A. Lyberatos, D. V. Berkov, and R. W. Chantrell, *J. Phys. Condens. Matter* **5**, 8911 (1993).
- ²⁶S. Maekawa, *Concepts in Spin Electronics* (Oxford University Press, London, 2006).
- ²⁷S. Takahashi and S. Maekawa, *Sci. Tech. Adv. Mater.* **9**, 014105 (2008).
- ²⁸N. Vernier, D. A. Allwood, D. Atkinson, M. D. Cooke, and R. P. Cowburn, *Europhys. Lett.* **65**, 526 (2004).
- ²⁹B. D. Cullity and C. D. Graham, *Introduction to Magnetic Materials* (Wiley, New York, 2009).
- ³⁰A. Lyberatos and J. Ferre, *J. Phys. D* **33**, 1060 (2000).
- ³¹K. Fukumoto, W. Kuch, J. Vogel, F. Romanens, S. Pizzini, J. Camarero, M. Bonfim, and J. Kirschner, *Phys. Rev. Lett.* **96**, 097204 (2006).
- ³²M. Tsoi, J. Z. Sun, M. J. Rooks, R. H. Koch, and S. S. P. Parkin, *Phys. Rev. B* **69**, 100406 (2004).